Grid turbulence studied by Particle Image Velocimetry

Daniel Duda[1,*], *Jindřich* Bém[1], *Vitalii* Yanovych[1], and *Václav* Uruba[1,2]

[1]Faculty of Mechanical Engineering, University of West Bohemia, Pilsen, Czech Republic
[2]Institute of Thermomechanics, Czech Academy of Sciences, Prague, Czech Republic

Abstract. We studied the grid-generated turbulence by using Particle Image Velocimetry (PIV) technique. We test on this already well studied flow the new ways of analyzing spatially resolved PIV data, such as the spatial spectra and structure functions. We compare some of the turbulence characteristics with results of Laser Doppler Anemometry (LDA).

1 Introduction

The decay of turbulence produced by flow passing a regular grid is a standard turbulence problem [1–6]. The grid turbulence is interesting from the theoretical point of view as it is a prototype of an „ideal“ Kolmogorov-type turbulence, which is homogeneous and isotropic (of course, it is not fully true) [3, 7]. It decays in space, but from the point of view of the fluid, it decays in time. The decay realizes via the Richardson cascade, which transports the energy into both: smaller and larger scales. The energy at smallest scale, called Kolmogorov scale, dissipates due to viscosity and, as there is no other energy input than the transfer from larger scales, the turbulence decays from bottom: growing the Kolmogorov scale.

This flow has been studied experimentally many times by using mainly the *Hot Wire Anemometry* (HWA) [8], which is the method best suitable for turbulence research. Its result is a perfect time-series of velocities in *single point*.

In this study we use another widely used experimental method: *Particle Image Velocimetry* (PIV) [8, 9]. It is based on direct optical observation of small particles (or droplets) carried by the fluid in the entire field of view of a camera. This method has lower precision than the HWA, but it offers the spatially resolved instantaneous velocity fields, which is the aspect, we found to be crucial to distinguish the main building blocks of turbulence – vortices [10–12].

This investigation of already a well-studied flow focuses to testing new ways of analysis of the spatially resolved PIV data. We used the LDA (Laser Doppler Anemometry) technique as well, which offers higher accuracy, but only in one point. Therefore we compare turbulence characteristics such as turbulence intensity obtained by both techniques. More details can be found in our previous publication [13].

2 Experimental setup

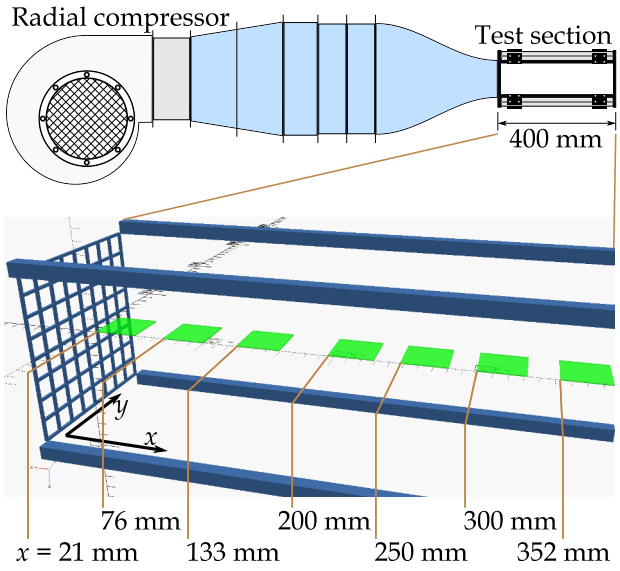

Fig. 1. Sketch of the wind tunnel (top) and the position of the studied areas in respect to the grid, which is located at the inlet into the transparent test section.

The flow has been generated by WT-tech wind tunnel of maximum achieved velocity 25 m/s (this experiment) with the transparent test-section of size $125 \times 125 \times 400$ mm. At the beginning of the test section, there is the grid with grid spacing $M = 125\,\text{mm}/8 = 15,625\,\text{mm}$, thickness of square rods is $d = 2$ mm, therefore the porosity $\beta = (M - d)^2/M^2 = 76\%$.

PIV measurement is performed by using a commercially available Dantec PIV system. Illumination is realized by a double-pulse Nd:YAG solid-state laser

*e-mail: dudad@kke.zcu.cz

NewWave Solo which produces a pair of 500 mJ shots lasting 5 ns. Double-frame CCD cameras FlowSense MkII can distinguish two expositions separated by only $1,5\,\mu$s, but the repetition frequency does not exceed $7,4$ Hz, thus the obtained instantaneous velocity fields can be considered as statistically independent. As the tracer particles we use droplets of $\sim\ \mu$m diameter produced by commercially available fog generator SAFEX.

We have measured the flow in 7 square areas of size 32×32 mm, i.e. $\sim 2M$, located 21, 76, 133, 200, 250, 300 and 352 mm from the grid (this is the location of the leading edge of these areas). Their z-coordinate is $7,5$ mm under the axis of the test section, which is approximately close to the middle of the first grid hole. We have measured at velocities u ranging from $1,2$ to 25 m/s. M-based Reynolds number $Re = u \cdot M/\nu$, where ν is the kinematic viscosity of air. Re ranges from $1,3 \cdot 10^3$ to $2,7 \cdot 10^4$.

3 Results

General description of the grid turbulence is that, the turbulence is first produced by the interacting jets behind the holes, or by interacting the wakes behind the rods, as is apparent in figure 2(a). Wakes are widening as described e.g. by [14] – note the double maxima of TKE at small distance (Fig. 3(a)), at later stage (Fig. 3(b)), the pair of maxima is separated more than the maxima produced by neighboring rods. Even later, it starts to be influenced by the horizontal rods up and down the measuring plane.

3.1 Turbulent kinetic energy

Turbulent kinetic energy (TKE, K) is average kinetic energy associated with vortices and other coherent flow structures, which the turbulence consists of. It is calculated as *variance* of velocity, i.e.

$$K\left(\vec{x}\right) = \frac{1}{2}\left(\left\langle u^2\left(\vec{x}\right) + v^2\left(\vec{x}\right)\right\rangle_T - \left\langle u\left(\vec{x}\right)\right\rangle_T^2 - \left\langle v\left(\vec{x}\right)\right\rangle_T^2\right) \quad (1)$$

Where u and v denote the x- and y-component of the velocity vector, $\vec{x}$ is location and $\langle\cdot\rangle_T$ denote the averaging over time, i.e the ensemble averaging in this case of relatively „slow“ PIV.

The flow is naturally three-dimensional, while we have measured only the planar cut, therefore we lack any information about the third velocity component w. Some authors solve this issue by assuming that the third component fluctuations are statistically equal to the second component (v), thus they multiply that term by two. We prefer to keep the measured data and not to introduce more artificial assumptions, than it is needed.

Equation (1) can be rewritten by using the energies of instantaneous velocity field E and of averaged velocity field E_T as $K = E - E_T$, where $E = \frac{1}{2}\left\langle \vec{u}^2\right\rangle_T$ and $E_T = \frac{1}{2}\left\langle \vec{u}\right\rangle_T^2$.

The spatial distribution of TKE at first three positions is plotted in figure 3, the rest is no more interesting, because the spatial distribution is flat in span-wise direction (y). The change of the amount of TKE in stream-wise direction (x) is better recognizable in figure 4, where the average over y of TKE is displayed. When we take into account only the data more far away from the grid, we find the decay with power -1.95. Note that this value can differ, when we would use an *virtual origin*, i.e. shifting of x by some x_0, which is used by some authors [2]. In article [13], we have shown, that the decay exponent depends on the length-scale as well. TKE of small scale decays faster at small Reynolds numbers, while at large Re, the decay rate is same for all scales (Figure 8 in [13]).

The value of TKE is underestimated when measured by using the PIV method, because this method assumes a homogeneous motion inside the so-called *interrogation area*, whose size is 0.51 mm in our case. Thus all flow structures smaller than this size are neglected and does not counted in our TKE. On the other hand, the majority of energy occurs at larger scales due to the quite steep decay of power spectral density, which is (in the homogeneous and isotropic turbulence) $-5/3$. Thus we need to test our result by another method more sensitive even to the small scale, which is the Laser Doppler Anemometry (LDA).

3.2 Comparison with Laser Doppler Anemometry

Laser Doppler Anemometry (LDA) measures the velocity of small particles caried by the fluid (similarly as PIV does) in a one small volume, where two coherent laser beams cross. The size of this measurement volume is around $xx\,\mu\text{m}^3$, thus it can be considered as a point. LDA is generally though to be a precise trustworthy absolute method, which is limited only by the ability of used tracer particles to follow the flow.

We measured the stream-wise velocity u and compared the results obtained by both techniques, as shown in figure 5. The value of stream-wise velocity strongly depends on the position, specially in the vicinity to the grid. Generally, speaking, the flow is accelerated in the jets and decelerated in the wakes behind the rods. The measurement point of LDA has been located into the wake. Therefore for comparison with PIV, we have to select the cut from the wake, as it is done in figure 5. There are plotted also PIV data averaged over the span-wise direction, thus containing both, jets and wakes. The data plotted in figure 5 suggest that the LDA measuring point has not been exactly in the wake, as its position has been selected manually before the measurement, while the track of the wake in PIV data has been selected after the measurement from the data. This difference vanishes in higher distances from the grid.

The plot of standard deviation $\sigma_T[u]$

$$\sigma_T[u] = \sqrt{\left\langle u^2 - \langle u\rangle_T^2\right\rangle_T} \quad (2)$$

shows better agreement between LDA and PIV data from the rod wake. The standard deviation in LDA data is systematically higher by about 13%. It is too much to have only physical reasons discussed above, it can partly be caused by non-identical coordinate systems in LDA and PIV data. This issue we will fix in future by using an motorized traverser for the LDA measuring head.

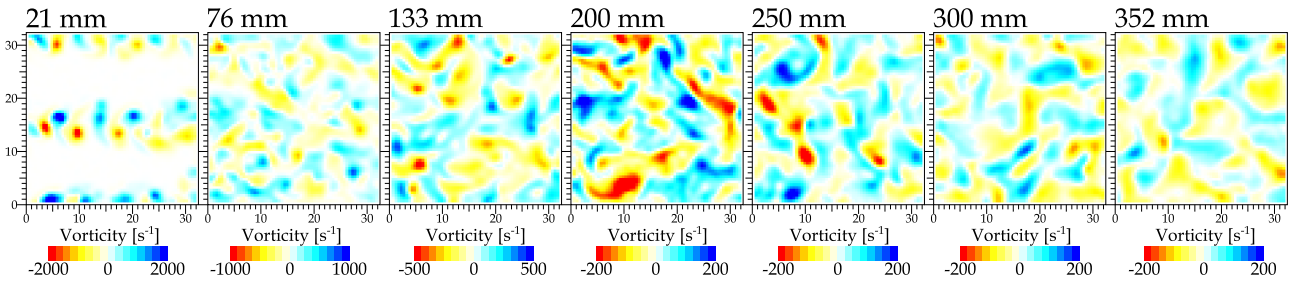

Fig. 2. Examples of spatial distribution of instantaneous vorticity ω in 7 studied areas (see figure 1). Stream-wise velocity (from left to right) is 3.0 m/s corresponding to Reynolds number $Re = 3.1 \cdot 10^3$. Note the different color-scale of first three images.

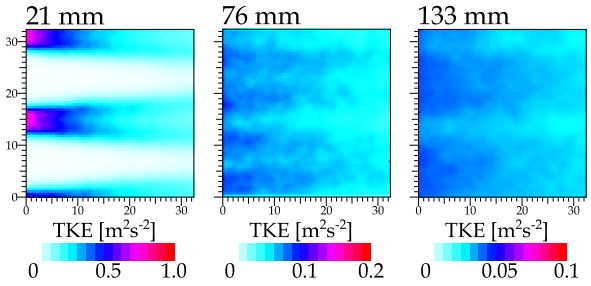

Fig. 3. Spatial distribution of the turbulent kinetic energy. Stream-wise velocity is 3.0 m/s, corresponding $Re = 3.1 \cdot 10^3$.

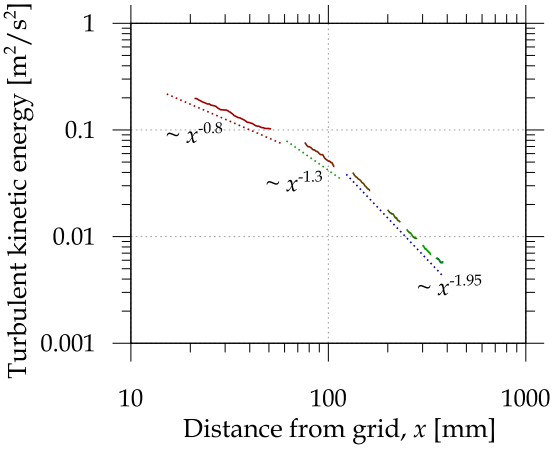

Fig. 4. Turbulent kinetic energy as a function of the distance from the grid for Reynolds number $3.1 \cdot 10^3$. The plotted value is averaged over the span-wise coordinate (y). There are displayed powers of the dotted lines just under the data (solid lines). Note the log-log plot.

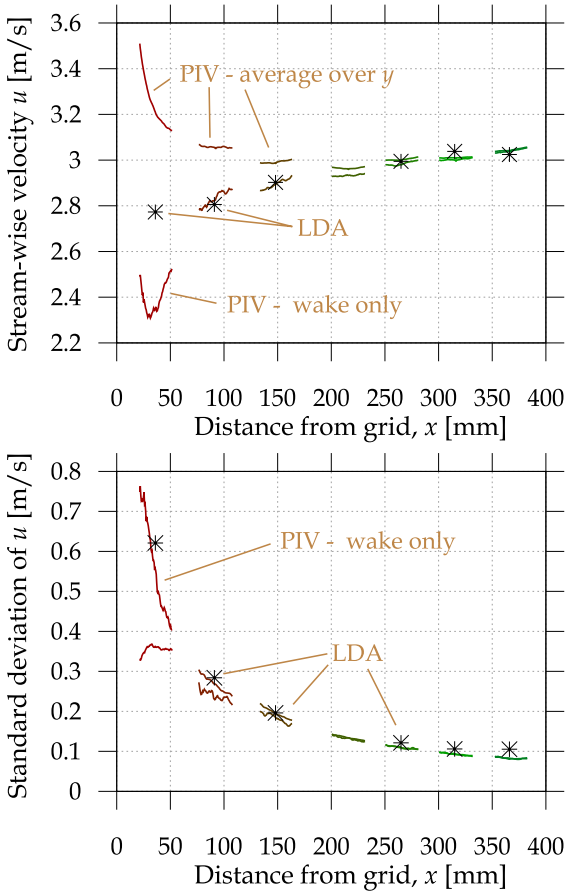

Fig. 5. Top: Stream-wise velocity u measured by using PIV (solid lines) and LDA (stars). The PIV data is processed by 2 ways: it is averaged over the span-wise direction (y) or there is selected only a single profile in the wake of the grid rod. **Bottom**: Standard deviation of the stream-wise velocity. This is plotted instead of TKE, which needs all three velocity component, while our LDA system measures only one component. Again, the PIV data are selected to the averaged ones and those from the wake only, which gives highest difference at locations close to the grid.

3.3 Intensity of turbulence

The turbulence produces at the grid and later on it dissipates according to a power law, which is shown in figure 4 for one velocity. The PIV offers two ways of defining the turbulence intensity, which is a quantity useful for describing the decay processes: the classical definition based on the temporal averaging we denote I_T and we calculate it as

$$I_T = \frac{(E - E_T)^{1/2}}{E_T^{1/2}} \qquad (3)$$

, where $E = \frac{1}{2}\vec{u}^2$ is the average energy of instantaneous velocities, while E_T is the energy of temporal average velocity, $E_T = \frac{1}{2}\langle\vec{u}\rangle_T^2$. This turbulence intensity does not contain the spatial changes inside the average velocity field, such as the wakes or jet structures. Therefore we can use an alternative definition of spatial intensity of turbulence

I_P calculated similarly as

$$I_P = \frac{(E - E_P)^{1/2}}{E_P^{1/2}} \tag{4}$$

, where the subscript P plays for spatial averaging, i.e. averaging over the field of view. In principle, this quantity can be calculated by using a single instantaneous velocity field only. The effect is evident in figure 6, where close to the grid, the spatial intensity is larger due to the structure even in the averaged velocity field (the mentioned jets and wakes), while more far from the grid, the temporal one is grater due to the fluctuations larger than the investigated field of view as the integral length-scale grows.

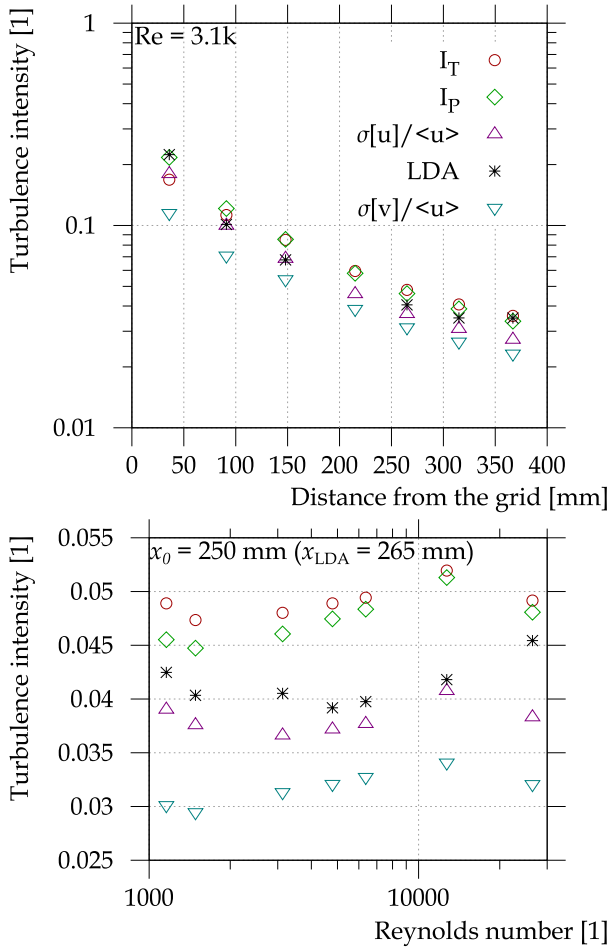

Fig. 6. Top: intensity of turbulence obtained by using different approaches as a function of distance from the grid. The Reynolds number is $3.1 \cdot 10^3$. **Bottom**: intensities of turbulence as a function of Reynolds number at constant mean distance from the grid $x_0 = 250\,\text{mm} = 16M$, $x_{\text{center}} = 265\,\text{mm} = 17M$. I_T and I_P reflects the temporal and spatial intensity calculated according to equations (3) and (4) respectively, The data obtained from LDA, which measures x-component only, can be compared only with the stream-wise turbulence intensity $\sigma[u]/\langle u\rangle$. For complexity, there is also plotted the span-wise component $\sigma[v]/\langle u\rangle$, which is normalized by stream-wise velocity, as the mean value of span-wise velocity is close to zero.

The comparison with LDA data can be done only for the corresponding quantity, which is the ratio of standard deviation of stream-wise velocity and its average value, as this is the component, which is measured. This quantity obtained from PIV data is displayed in figure 6 as well. As this contains only fluctuations in one direction, its value is naturally lower, than that containing both measured components (and if we would have measured the third component as well, the value might be even larger). On the other hand, it is evident, that, again as discussed above, the PIV slightly underestimates the fluctuations.

3.4 Length-scale dependent fluctuations

The idea of averaging over space instead of over time can be broaden by using different length scales of averaging than just the entire field of view. We can focus on spatial fluctuations in respect to different vicinity of the probed point. This can be done by convoluting the velocity field $\vec{u}(\vec{x})$ with band-pass filter [15], which consists of two Gaussian functions:

$$\vec{u}_{lh}(\vec{x}) = \vec{u}(\vec{x}) * \left(\frac{1}{2\pi\sigma_l^2} e^{-\frac{x^2}{2\sigma_l^2}} - \frac{1}{2\pi\sigma_h^2} e^{-\frac{x^2}{2\sigma_h^2}} \right) \tag{5}$$

The resulting velocity field $\vec{u}_{lh}(\vec{x})$ is smoother than the lower bound σ_l and rougher than the upper bound σ_h, thus it contains only fluctuations of specific length-size interval. The process is illustrated in figure 7.

When we have the velocity fields with highlighted different scale of fluctuations [16], we calculate the TKE of each ensemble getting the spatial distribution of each interval of length-scales [17]. Then we select three of this intervals and combine them into a single image. The red channel comes from the small length-scale, i.e. $\sigma_l^R = 0.5\,\text{mm}$ and $\sigma_h^R = 0.7\,\text{mm}$, the green channel does from the middle scales, i.e. $\sigma_l^G = 1.5\,\text{mm}$, $\sigma_h^G = 2.0\,\text{mm}$ and the largest scales are coded into blue channel, i.e. $\sigma_l^B = 3.9\,\text{mm}$ and $\sigma_h^B = 5.9\,\text{mm}$. The relative magnitude of colors is weighted according to the *thickness* of the interval and to the estimated Kolmogorov scaling (thus that the ideal homogeneous and isotropic turbulence would be displayed in gray-scale).

3.5 Spatial spectrum

By using this approach we can obtain the spatial spectrum as a plot of standard deviation of energies of a band-pass filtered velocity field in dependence on the effective wave vector of the band. Figure 8 shows the resulting spectra, first in dependence on the distance from the grid for constant velocity (i.e. *Re*), second, in dependence on velocity for constant distance from the grid.

The spectrum is already smoothed, which is in consistency with the general uncertainty principle: the particular localization in direct space is redeemed by delocalization in the Fourier space. Additionally, the available range is quite short: we are limited from one side by the size of the measuring grid, which is 0.5 mm, from the other side by the size of the largest σ_h, which is 5.9 mm. One can ask, why not by the size of field of view, which is around 5× larger. This is due to the fact, that the real size of the

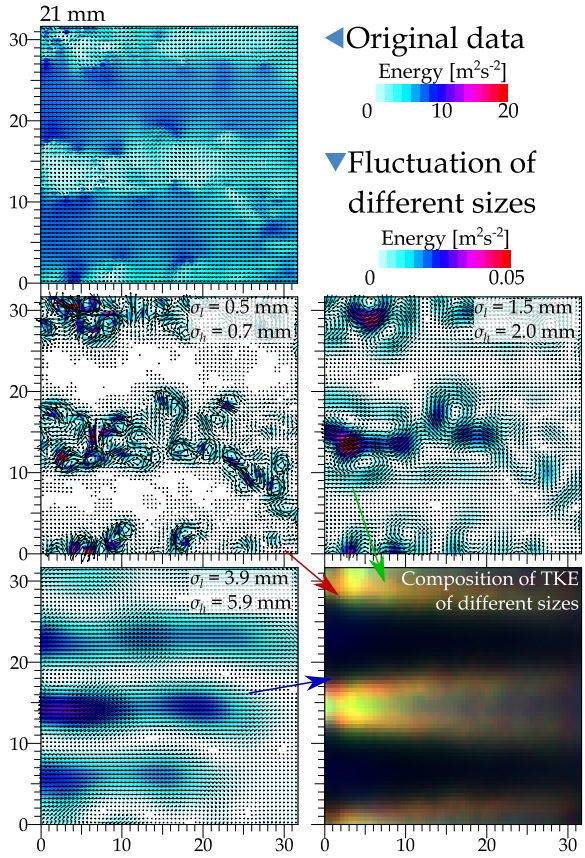

Fig. 7. Top left: example of the instantaneous velocity field colored by the energy (i.e. half of square of velocity magnitude). **Middle left**: the same data with highlighted fluctuations of size interval from $\sigma_l = 0.5$ to $\sigma_h = 0.7$ mm. **Middle right**: from $\sigma_l = 1.5$ to $\sigma_h = 2.0$ mm. **Bottom left**: from $\sigma_l = 3.9$ to $\sigma_h = 5.9$ mm. **Bottom right**: Length-scale dependent fluctuations, red colors correspond to smallest length-scales, green to middle scales and blue to largest scales. The Reynolds number is $3.1 \cdot 10^3$, the left side of the panels is 21 mm from the grid.

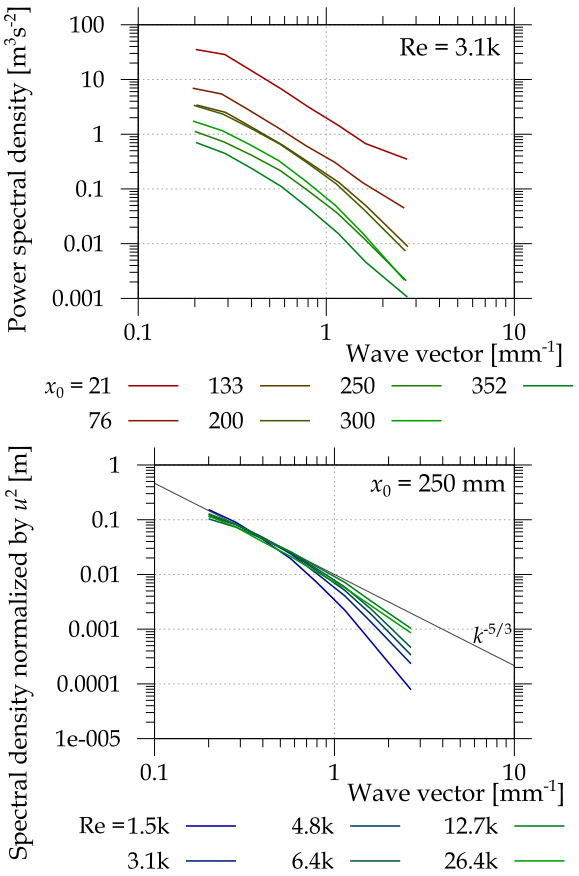

Fig. 8. Top: The power spectral density as a function of the distance from the grid (the x_0 means the leading side of the probed areas) at constant Reynolds number $Re = 3.1 \cdot 10^3$. **Bottom**: the power spectral density divided by square of velocity as a function of Reynolds number at constant distance from the gird $x_0 = 250\,\text{mm} = 16M$. For comparison there is plotted the famous Kolmogorov $-5/3$ law.

effective support of the band pass is much larger than its half-width, therefore the value in such a point is already influenced by too many points lying outside of the measured field of view. We want to minimize the boundary effect of the points outside, whose value is extrapolated by using the „Extend Edge Handling“ approach (i.e. that the nearest border points are conceptually extended as far as necessary to provide values for the convolution. Corner points are extended in 90° wedges. Other edge points are extended in lines).

As the spectrum is spatial, it is questionable, if it makes sense close to the grid, where the flow contains strong structures even in the average, as are jets and wakes produced by the grid rods. The spatial spectrum naturally mix the data from both very different regions and thus its physical interpretation is not easy. On the other hand, the fact, that the spectrum close to grid is despite the just mentioned reason very similar to the others, suggests that the famous Kolmogorov law developed for homogeneous and isotropic turbulence has more mathematical than physical reasons, because it should *not* be valid in that case.

The dependence on Reynolds number (Figure 8 bottom) shows that at lower velocities, the spectrum falls down faster than the Kolmogorov scaling suggesting the vicinity of the Kolmogorov scale in that distance.

The power spectral density shown in figure 8 bottom is normalized by the square of the mean stream-wise velocity. Note, that the lines meet at the larger scales, which again suggest, that the energy normalization follows these larger scales, while the energy deficit (towards the ideal Kolmogorov profile) does not affect the overall mean velocity.

3.6 Structure functions of second order

The structure function [18] of second order of the stream-wise velocity component u is defined as

$$S^2_{uu}\left(\vec{x},\vec{\xi}\right) = \frac{\left\langle \left(u\left(\vec{x}\right) - u\left(\vec{\xi}\right)\right)^2 \right\rangle_T}{\sigma_T\left[u\left(\vec{x}\right)\right] \cdot \sigma_T\left[u\left(\vec{\xi}\right)\right]} \tag{6}$$

where $\vec{x}$ denote the probed point, where the structure function is calculated, while $\vec{\xi}$ is the reference point; σ_T means

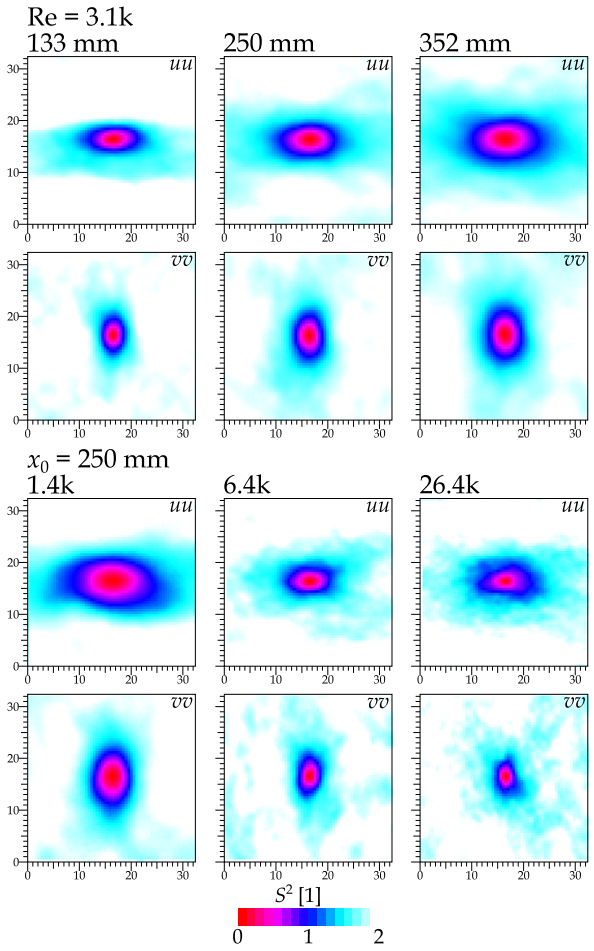

Fig. 9. Top: spatial distribution of the structure function around the point $\vec{\xi}$ in the center of the field of view in different distances from the grid. The first line shows the structure function of u, i.e. x-component of the velocity, second line does the v, which is the span-wise component. The velocity is constant corresponding to $Re = 3.1 \cdot 10^3$. **Bottom**: the distance from the grid is constant and equals to $x_0 = 250$ mm, different panels show different Reynolds numbers.

the standard deviation (2) in respect to time, i.e. ensemble in this case of relatively slow PIV. S^2_{uu} thus says, how much is the value of u at the point $\vec{x}$ statistically related to the value of u at point $\vec{\xi}$. When the values are same (which is identically fulfilled when $\vec{x} = \vec{\xi}$), the value of $S^2 = 0$, when the values are not correlated, the value of $S^2 = 2$.

As has been proven in [18], the S^2 is in close relation to the autocorrelation function C_{uu} as $S^2_{uu} = 2-2C_{uu}$, when the sample size is infinite. But, in respect to autocorrelation function, the structure function is not sensitive to the mean value and it converges better.

Analogically to the equation (6) we can define S^2_{vv} for the span-wise velocity component v:

$$S^2_{vv}\left(\vec{x},\vec{\xi}\right) = \frac{\left\langle \left(v\left(\vec{x}\right) - v\left(\vec{\xi}\right)\right)^2 \right\rangle_T}{\sigma_T\left[v\left(\vec{x}\right)\right] \cdot \sigma_T\left[v\left(\vec{\xi}\right)\right]} \qquad (7)$$

These functions are autostructure functions as they probe the same quantity only in different locations. There can be defined also a crossstructure function S_{uv}, which we do not discuss in this article.

Spatial distribution of both functions is plotted in figure 9, first for different distances from the grid at constant velocity, second for different velocities at constant position. In all cases is the reference point $\vec{\xi}$ chosen in the center of the field of view.

In all panels of figure 9 we can see that the distribution is not axially symmetric, e.g. the difference between values of stream-wise velocity grows faster in span-wise direction than in the stream-wise one, which suggests that the turbulence is not isotropic even in this quite large distances from the grid. In addition, this anisotropy does not seems do decrease with distance from the grid.

The range of the similar points grows with increasing distance as can be estimated from the fact, that the turbulence decays from bottom (i.e. the Kolmogorov dissipative scale grows). This range decreases with increasing Reynolds number, as can be seen in the bottom half of figure 9.

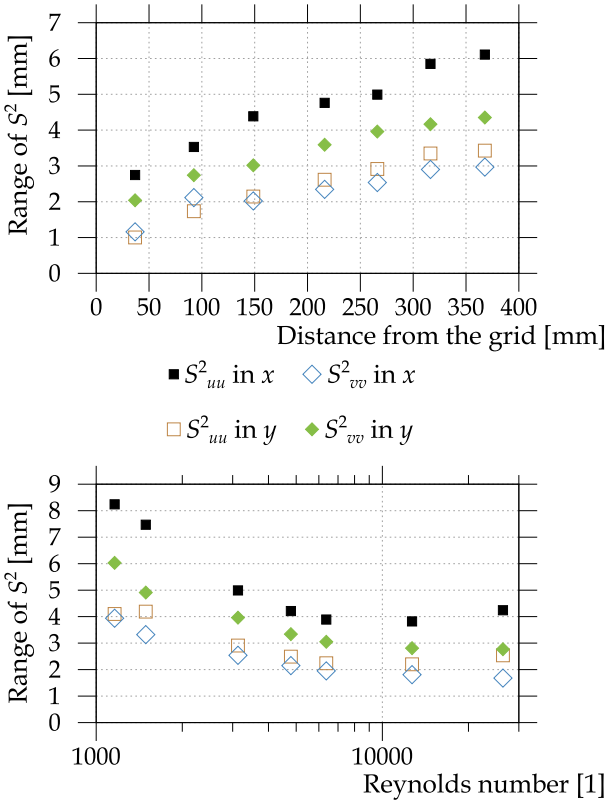

Fig. 10. Top: Range of structure function S^2. The velocity is constant corresponding to $Re = 3.1 \cdot 10^3$. **Bottom**: the distance from the grid is constant and equals to $x_0 = 250$ mm.

We try to quantify the range R of structure function as a distance of the reference point $\vec{\xi}$ to point, where $S^2 = 1$, in some important direction, which is the stream-wise or the span-wise direction. The result is plotted in figure 10.

Again, we see, that the range of structure function increases with distance from the grid and decreases with velocity. In the first dependence we can see an interesting *slowing of increase* around distance 200 mm; this effect is

probably connected with the lost of averaged large-scale structure of alternating jets and wakes. On the other hand, the decrease with velocity is not fully uniform, as can be seen at the highest velocities in the bottom part of figure 10. At this moment, we doubt that this effect was physical; we prefer the hypothesis, that it is an error of PIV measurement technique connected with higher velocities. In the future we plan to perform a similar comparison with LDA data, as it has been done above for the turbulence intensity, but we are not yet familiar with the LDA processing software.

4 Conclusion

The grid-generated turbulence has been studied by using both, PIV and LDA techniques. We observe that both methods give similar results, mainly at lower velocities. At higher velocities the PIV technique underestimate the fluctuations, probably due to the finite size of the *interrogative area*, inside which the velocity is averaged.

The turbulent kinetic energy decays with distance as $x^{-1.95}$.

We used a new method of spatial turbulence spectra [17] and we have found that they follow the Kolmogorov law even in the vicinity of the grid, where the turbulence is not homogeneous neither isotropic. At smaller velocities, we observed a deviation from this law caused probably by the vicinity of the dissipative length-scale.

Structure functions show that the turbulence is surprisingly not isotropic as the shape of the structure function is deformed in the direction of the flow (it is prolate in the axis of the investigated velocity component). The range of structure function increases with distance and decreases with velocity, although there is an inexplicable increase at largest velocity, which might be an PIV artifact, but we lack the comparison with LDA to proof that at this moment.

Acknowledgements We thank to Václav Koudelka and Karsten Dörner from Dantec Dynamics for valuable technical help with the LDA system. This work was supported by the project of Technology Agency of the Czech Republic TAČR No TH02020057 „Program Epsilon“.

References

[1] T. Kurian, J.H.M. Fransson, Fluid Dynamics Research **41**, 021403 (2009)
[2] M. Mohamed, J. LaRue, J. Fluid Mech. **219**, 195 (1990)
[3] P. Roach, International Journal of Heat and Fluid Flow **8**, 82 (1987)
[4] G. Comte-Bellot, S. Corrsin, J. Fluid Mech. **25**, 657 (1966)
[5] Z. Warhaft, J.L. Lumley, J. Fluid Mech. **88**, 659 (1978)
[6] W.Z. Grzelak J., TRANSACTIONS OF THE INSTITUTE OF FLUID-FLOW MACHINERY **130**, 93 (2015)
[7] S.B. Pope, *Turbulent flows* (Cambridge University Press, Cambridge, UK, 2000)
[8] C. Tropea, A. Yarin, J.F. Foss, *Springer Handbook of Experimental Fluid Mechanics* (Springer, Heidelberg, DE, 2007)
[9] D. Jašíková, M. Kotek, R. Horálek, J. Horčička, V. Kopeckỳ, ILASS – Europe 2010, 23rd Annual Conference on Liquid Atomization and Spray Systems, Brno, Czech Republic, September 2010 **23** (2010)
[10] D. Duda, J. Bém, V. Yanovych, P. Pavlíček, V. Uruba, European Journal of Mechanics, B/Fluids **79**, 444 (2020)
[11] D. Duda, in *Vortex Dynamics – From Physical to Mathematical Aspects [Working Title]*, edited by I. Bakırtaş, N. Antar (IntechOpen, 2021)
[12] D. Duda, *Individual vortex searching algorithm*, in *In Proceedings Topical Problems of Fluid Mechanics 2020*, edited by D. Šimurda, T. Bodnár (2020), pp. 56–63
[13] D. Duda, V. Yanovych, V. Uruba, Processes **8**, 1355 (2020)
[14] D. Duda, V. Yanovych, V. Uruba, Energies **14**, 4712 (2021)
[15] A. Agrawal, Experiments in Fluids **39**, 836 (2005)
[16] D. Duda, V. Uruba, AIP conference proceedings **2000**, 020005 (2018)
[17] D. Duda, V. Uruba, ASME J of Nuclear Rad Sci. **5** (2019)
[18] E.O. Schulz-DuBois, I. Rehberg, Applied physics **24**, 323 (1981)